Proceedings of ASME Turbo Expo 2011
GT2011
June 6-10, 2011, Vancouver, British Columbia, Canada

GT2011-45393

EXPERIMENTAL AND COMPUTATIONAL RESULTS OF DISTRIBUTED COMBUSTION FOR APPLICATION IN CURRENT GAS TURBINE ENGINE COMBUSTOR ARCHITECTURES

Nick Overman and Jason Ryon
Goodrich Engine Components
West Des Moines, IA, USA

ABSTRACT

Current development and testing has lead to a fuel/air injection system for application in gas turbine engines that produces ultra low emissions and stable, lean combustion. The system is designed to operate with current combustor architectures similar to existing gas turbine engines. This paper presents both experimental and numerical test results demonstrating the benefits of such technology including extremely low emissions of NO_X, CO, and un-burned hydrocarbons (UHC). Primary focus is on experimental results demonstrating reaction distribution and emissions. Numerical confirmation of flow field dynamics was used to develop an understanding of the re-circulation rates within the combustor and impact on reaction behavior. Several design configurations were tested to investigate the effects of aerodynamic stagnation point and fuel placement with respect to the aerodynamic shear layer produced by the swirling flow field. Test conditions were varied, including inlet air temperature and injector pressure drop for monitoring effects on the operating envelope of distributed reaction and on lean blow out limit. Results demonstrate the improved performance of a system capable of operating in a flameless or distributed reaction mode over that of a typical lean burn system.

INTRODUCTION

Over the last five years there has been a great amount of interest raised across the gas turbine engine (GTE) community concerning the application of flameless combustion for gas turbine engines for its high combustion efficiency, low emissions, excellent stability, low noise, homogeneous temperature pattern, and lower fuel sensitivity. The term flameless was coined from the phenomena in which a lean mode of combustion can be achieved for which the flame becomes invisible to the naked eye. Originally, this mode of combustion was discovered in developing advanced industrial furnaces several years ago. The flameless mode of combustion is a distributed volumetric reaction opposed to diffusion or turbulent eddy flames that are used in current gas turbine engines. For current gas turbine combustion, reactions occur in thin folded sheets such that the combustion is actually composed of many small folded surface reactions. The flameless or distributed reaction is a true volumetric reaction that has several benefits over current lean burn systems.

A turbulent eddy flame requires a flow stagnation point to anchor, whether it be by bluff body or aerodynamically driven. This form of stabilization is susceptible to thermo-acoustic instabilities as the stagnation point can be perturbed by oscillations in either aerodynamic or heat release effects. When this occurs coupling between thermal, acoustic, and aerodynamic oscillations result, which in turn amplify the instability to levels capable of causing critical failure in an engine. In a distributed reaction there is no single anchor point, so perturbations in combustion or in the stagnation point do not couple. This prevents the formation of large amplitude instabilities. Subsequently the combustion is also quieter than current GTE technology, which should help these engines meet stricter noise requirements. Current methods of combustion have encountered difficulties maintaining stability as combustor inlet pressures and temperatures rise, and therefore they are relying more on passive methods of reducing these instabilities in addition to considering active control systems to suppress instabilities. These instability reduction methods add weight and complexity to engines. Designing combustion systems capable of flameless combustion is a means of overcoming instabilities without adding extra weight, complexity, and cost.

Another benefit of the distributed reaction is in emissions, as this mode of combustion is capable of reducing both carbon monoxide (CO) and oxides of nitrogen (NO_X) to levels below 5 − 10ppm simultaneously with virtually no unburned hydrocarbons (UHC). This is achieved through the combustion chemistry and does not require adding steam to the reaction zone, or post treating exhaust gases to achieve these extremely low emission levels. This is an advantage over current low emission ground based systems that require water injection and/or large expensive catalysts for exhaust gas treatment that add size, cost, and complexity.

The fuel/air injection system discussed in this paper utilizes strong swirl to internally recuperate heat, while all air and fuel enters the combustor through the device and without addition from dilution holes found in traditional systems. In the system tested there was no film cooling air which may be possible in advance ceramic matrix combustors. However, in this case the elimination of film cooling is not out of necessity, but rather simplicity because it is not needed.

The focus of this paper is to disclose some of the test results and demonstrate an injector capable of producing distributed combustion within a traditional GTE combustor architecture using diesel fuel. This differs from the majority of work done in this field to date that has relied on varying incarnations of reverse flow combustors (Arghode, Gupta [1], Zin et al. [8]), re-circulation of combustion products outside of the combustion zone (Milani, Wünning [4]), dual combustors in series (Hamdi [5]), and/or gaseous fuels to achieve distributed reaction.

NOMENCLATURE

Variables

CO = Carbon monoxide
CO_2 = Carbon dioxide
D = Combustor diameter
GTE = Gas turbine engine
ℓ = Axial distance from combustor dome
LBO = Lean blow out
N = Number of moles (kmol)
NO_X = Oxides of nitrogen
O_2 = Oxygen
UHC = Unburned hydrocarbons
x = Number of carbon atoms in molecule of fuel
y = Number hydrogen atoms in molecule of fuel
ΔP = Pressure difference
$\phi = \frac{\left(\frac{A}{F}\right)_{STOICH}}{\left(\frac{A}{F}\right)_{ACT}}$ = Equivalence ratio
χ = Mole fraction (kmol/kmol)

Subscripts

act = Actual measured value
corr = Corrected value
LBO = Lean blow out
mix = Value for total exhaust mixture
stoich = Stoichiometric value
3 = Condition upstream of injector (compressor discharge)
4 = Condition at combustor

SYSTEM DESCRIPTION

The device tested was designed primarily for application in can-annular style ground based gas turbine engines for power generation, though its use is not necessarily limited to only this application. For experimentation the combustor was simulated with a simple quartz tube that allowed optical access for measurement and visualization purposes. The primary design changes for achieving flameless are all done within the fuel/air injection and mixing device upstream of the combustor. This differs from some other flameless combustion systems that effect engine architecture, such as reverse flow combustors that use rectangular [1] or elliptical [2] combustors, or concentric flow with central stagnation point [11], or other systems that use heat exchange systems [9] for increasing inlet air temperatures. In this system all air is injected through the upstream fuel/air injector with no secondary or dilution air added as in traditional gas turbine combustors. This system does not use premixing, water injection, or catalyst for emission reduction. It does not use passive or active instability suppression devices.

The injection system consists of four independent fuel delivery circuits: primary and secondary fuel circuits for both liquid and gaseous fuels. Each fuel circuit delivers fuel to multiple fuel injection sites. Possessing two liquid and two gaseous fuel circuits allows significant flexibility in fuel usage. Though the injection device is installed upstream of the combustor as in current gas turbine architectures, it has features for re-circulating combustion gases upstream and internally to the device while mixing air, fuel, and combustion products in a manner which promotes distributed reaction within the combustor. Though flameless combustion only occurs at very lean conditions, the system performs well even up to stoichiometric conditions. From its operational characteristics comes the device's name of the Internal Re-circulating Lean Injector (I.R.L.I.). In this instance internal means internal to the combustor, not just internal to the engine. Since all air enters through the injection device it is almost solely responsible for establishing the downstream flow field structure within the confinement of the combustor.

Figure 1 is a depiction of the patent pending injection geometry which consists of an upstream swirl chamber with secondary swirler, followed by a convergent-divergent section, a primary swirler, and finally a divergent section. Fuel is injected at several circumferential locations near the upstream divergent-convergent section and within the divergent section downstream of the primary swirler. For the focus of this paper the only geometry variation was that of the primary and secondary swirlers. The ratio of effective area between the swirlers was varied while maintaining a constant total effective area. Table 1 outlines the difference in injector configurations that will be discussed in greater detail in a later section.

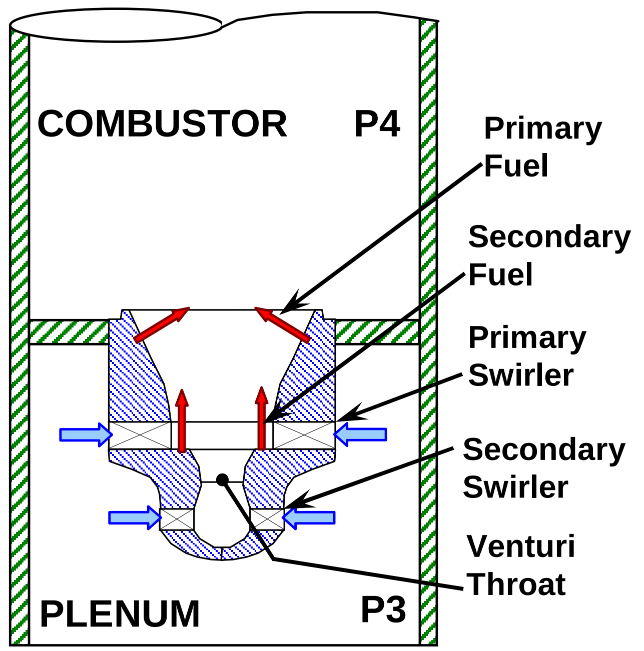

Figure 1: Injector Geometry. Cross Section sketch depicting injector geometry including primary and secondary injection of air and fuel, where there are multiple fuel injection sites around the injector circumference and where the location of fuel injection is the same for both liquid and gaseous fuels.

Configuration	Effective Area Ratio $\frac{\text{Primary Swirler}}{\text{Secondary Swirler}}$
IFH	3.92
PIFH	2.25
TFH	1.40

Table 1: Test Configuration. List of the injector configurations detailed in this paper, where the difference between configurations is the ratio of effective area of the primary swirler divided by the effective area of the secondary swirler, while the summation of the effective areas is constant.

In many ways the I.R.L.I. injector raises the possibility of reducing complexity in hardware, control, and exhaust treatment of a gas turbine engine. Additionally, safety is improved since the device does not pre-mix fuel and air as does many GTE combustion systems. These benefits can lead to reduced engine and operation costs.

EXPERIMENTAL SET-UP

Combustion testing was performed on an atmospheric vertical test stand, as seen in Figure 2, consists of a 72kW heater for preheating inlet air, a 24in (610mm) long, 5.25in (133mm) inner diameter flow conditioning segment containing a 16 gauge stainless steel perforated cone (40% open space), honeycomb straightener, and five screens: 20 mesh/45% open, 35 mesh/46% open, 40 mesh/42% open, and 165 mesh/38% open. Atop the flow conditioning section, is a 5.88in (149mm) long, 6.07in (154mm) inner diameter plenum section.

Figure 2: Experimental Set-up. Photograph showing the atmospheric test rig and combustor with measurement equipment at University of Cincinnati.

The vertical rig is supplied air through a 2in pipe supply line with a maximum pressure upstream of the air control valve of 100psig, allowing for up to 47.0lbm/hr (355g/s) air mass flow rate. The heater elements are able to safely reach a maximum temperature of 1400°F (760°C), but this temperature is limited by the mass flow rate of air passing through the heater. The maximum air mass flow rate used during these tests was 11.38lbm/min (86g/s), and the maximum air preheat temperature was 806°F (430°C).

Instrumentation ports are located near the exit of the flow conditioner, three of which are used for instrumentation to measure plenum conditions. Two ports contained sheathed-junction type K thermocouples, one for feedback control of the heater, and the second for data acquisition. The third port is used for a single Druck® pressure transducer with a 0-5 psig pressure range with a 1.0psig/V (6.89kPa/V) gain, and a 2.5 kHz response for measuring plenum pressure and pressure drop across the nozzle.

Various instruments were used for collecting experimental data during tests, including thermocouples, a microphone, fiber optics, and an intensified charge couple device (ICCD) camera. A Stanford Research Systems 16 channel thermocouple reader with 4 analog output channels was used to collect temperature data from type K thermocouples. The reader has ±1 of least significant displayed digit resolution (0.18°F (±0.1°C) for temperatures up to 1831.8°F (999.9°C), and ±1.8°F (±1.0°C) for temperatures 1832°F (1000°C) and higher) with automatic range select, and a 12Hz conversion rate.

A Brüel & Kjaer® low-noise high-sensitivity microphone was used for recording acoustic noise. The microphone was connected to a signal conditioner/variable amplifier set to a 0.1-10kHz dynamic range with a resolution of 6.89V/psi (1mV/Pa). The microphone was positioned such that it pointed toward the combustor exit from downstream of the combustor exit plane.

Three radial facing optical fibers were positioned outside the combustor pointed inward across the combustor approximately 2in (50.8mm) downstream of the dome plate. Fiber optic signals were conditioned through a photo-multiplier and a 310nm optic filter for measurement of OH.

An intensified charge coupled device (ICCD) camera with a 310nm optical filter was used to take images of the flame to indicate flame position and shape.

An emission sampling probe was used along the combustor exit plane to collect exhaust samples for emissions measurements. The California Analytical Instruments emission sensors measure NO_X, CO, CO_2, O_2, and unburned hydrocarbons (UHC), using model 601NDIR to measure CO, CO_2, and O_2, model 600CLD for NO_X, and model 300-HFID for UHC. Calibrated ranges for emissions were as follows: NO_X – 300ppm, CO – 300ppm, CO_2 – 20%, O_2 – 21%, UHC – 300ppm. The UHC sensor has a maximum resolution of 0.01ppm of carbon with 0.5% full scale repeatability with a response time of 90% full scale in 1.5sec. The NO_X sensor has a maximum resolution of 10ppb with repeatability better than 0.5% full scale with a response time of 90% full scale in less than 1sec. The $CO/CO_2/O_2$ has repeatability better than 1% full scale and a response time of 90% full scale in less than 2sec. Due to the length of the heated sampling line between the probe and sensors there is a 15sec delay between the time the sample is collected and the time it is measured. This delay is accounted for in post processing of the data so that emission concentrations correspond to the proper conditions recorded by the other instrumentation. Two different sampling probes were utilized, the first being a single point un-cooled ceramic tube set on a traverse unit for measuring emissions at discrete radial positions. The second probe was a double walled stainless steel multi-point probe used for collecting emissions at several points across the combustor exit plane simultaneously.

Multiple configurations of various injector sub-components were tested with combustion pressure near atmospheric. For each of these configurations several flow conditions were tested with air mass flow rates ranging between 437 - 682lbm/hr (55 - 86gm/sec), and preheat temperatures between 572 - 806°F (300 - 430°C), corresponding to injector pressure drops between 3 - 7%. Equivalence ratios tested ranged from ϕ = 0.8 to lean blow out (LBO), while fuel split varied such that the primary fuel circuit consisted of 17 - 95% of the total fuel flow.

EXPERIMENTAL RESULTS

Many injector configurations were studied but only three were down selected for representation in this paper. For all configurations the total effective area of the injector was relatively constant between 1.95 – 2.09in^2. The primary difference for the cases examined here is the ratio of effective areas between internal air circuits as shown in Table 1. In the first internal flame holding (IFH) configuration a re-circulation zone penetrates deep within the injection device with the propensity to pull the flame with it. This causes the flame to anchor within the mixing device itself and behave somewhat like a rich-quench-lean (RQL) system. Results are shown for this configuration using both gaseous propane and liquid diesel fuels. The second partial internal flame holding (PIFH) configuration allows for some internal anchoring but limits the amount of combustion products back flowing into the injector, resulting in a flame structure more indicative of current lean burn systems. The third transition flame holding (TFH) configuration reduces the penetration depth of the re-circulating flow into the device, resulting in a more distributed or flameless reaction where no single point acts as a flame anchor.

Table 2 illustrates the effect of stabilization method for each injector configuration on lean-blow-out (LBO). Lean-blow-out tests were performed by starting at an equivalence ratio between 0.7 – 1.0 and slowly reducing fuel flow while keeping airflow constant until flame extinction occurred. It is important to note that all air is passing through the injector, so there is no addition of cooling or dilution air that enters into the calculation of equivalence ratio (all air is for combustion). In contrast it is common place for lean burn or traditional combustion systems to take dilution and film cooling into account even when it does not necessarily take part in the combustion zone. The IFH configuration resulted in the lowest lean-blow-out limit. For gaseous propane this was as low as ϕ_{LBO} = 0.16, and for diesel ϕ_{LBO} = 0.22. The PIFH configuration showed had a significantly higher LBO limit, ϕ_{LBO} = 0.38, as the flame did not retreat into the device at lower equivalence ratios like the IFH configuration. Finally, the TFH configuration had the highest lean blow out limit of 0.43 for similar flow conditions. The LBO limit increases with pressure drop, as the increasing air velocity increases the shearing forces on the flame which result in earlier extinction, while increasing inlet temperature relieves this through faster chemical reaction rates. This configuration is labeled transitional flame holding as the method of flame anchoring transitions from an internal stagnation point to flameless mode of combustion without a single anchor point as the combustion becomes leaner.

Configuration	Fuel	T3 K	ΔP %	ϕ_{LBO}
IFH	Propane	593	3.20	0.16
IFH	Diesel	622	5.10	0.22
PIFH	Diesel	622	2.90	0.38
TFH	Diesel	572	3.00	0.43
TFH	Diesel	563	4.00	0.45
TFH	Diesel	676	3.80	0.37

Table 2: Lean-Blow-Out. Lower limit of flame extinction for different flame holding methods (injector configuration), fuel types, air preheat temperatures, and injector pressure drops.

As seen in Figure 3 the compressor discharge temperature (T_3) of typical gas turbine engines is generally above those air temperatures tested, while typical combustor pressure drops are between 2 – 4%. For the TFH configuration in Table 2, LBO decreases by 0.80 for a 113K increase in temperature. Though not shown other test cases follow this trend. Additionally, LBO consistently appears to increase with pressure drop. Therefore lean blow out limits achieved through testing may be conservative as higher inlet temperatures lead to lower lean blow out limits, though further testing will need to be conducted to determine the effects of increased combustion pressure on LBO.

Flame shape can be seen in the chemiluminescence images of Figures 4 – 6. The outlined white box in the images is the interrogation window for performing statistical analysis. For the chemiluminescence images the bottom white line corresponds to the combustor dome. The injector exit is centered at the lower bottom of the interrogation window with positive axial flow being upward. The right and left sides of the window correlate to the wall of the quartz combustor tube. The top of the window corresponds to the farthest downstream location that the reaction was observed in any of the test cases as determined through chemiluminescence. The images have been normalized so that the scale for each image is the same though the measured absolute intensity actually varied by two orders of magnitude between the rich and lean cases. For analysis purposes the lowest 10% of the intensity was filtered out to better determine the shape and volume of the flame.

The flame behavior of the internal flame holding (IFH) configuration can be seen in Figure 4. Only part of the flame can be seen in the combustion chamber, as a significant portion of the flame is contained within the injection device itself. As fuel flow rate is decreased (while maintaining air flow constant) the flame retreats toward the injector exit face. The flame continues to get leaner and is eventually pulled into the forward most swirl chamber upstream of the venturi throat, increasing the percentage of the reaction that completes within the device. The flame is held within the pocket of swirling air in the forward chamber allowing flame stability down to an overall equivalence ratio of about 0.16.

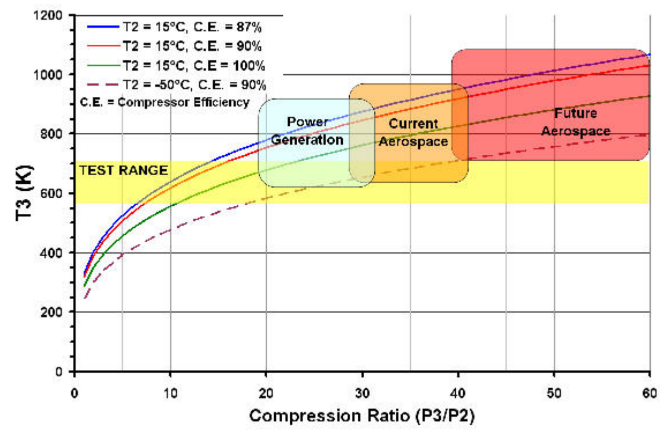

Figure 3: Compression Ratio verse Temperature. Plot showing GTE compressor discharge temperatures for ranges typical of industrial and aero gas turbine engines.

In contrast the partial internal flame holding (PIFH) configuration, as seen in Figure 5, does not retreat toward the injector face. Instead, as the equivalence ratio decreases the flame expands to fill the combustion chamber. However, the flame can still be seen as "rooted" within the injector such that the base of the flame is still held within the injector even lean blow out conditions. Though the combustion appears to be approaching a distributed mode at leaner condition, it never fully envelops the combustion zone due to the continued anchoring of the flame inside the injector.

The third, transitional flame holding (TFH) configuration yields a significantly different flame structure as seen in Figure 6. Instead of the concave shape near the injector face at near stoichiometric conditions, the flame is more convex: it appears to bulge toward the upstream dome plate opposed to pulling away like the other configurations. The flame also appears to broaden faster with downstream axial position from the injector face. At leaner conditions, approximately $\phi < 0.55$, the flame expands to fill the entire interrogation zone and by $\phi \approx 0.50$ fills over 99%. In contrast, at the leanest operating conditions, the reaction zone produced by the PIFH was only around 75% and the IFH was only 7% of the interrogation window. Similarly the standard deviation of flame intensity at the leanest condition as taken by the ICCD before LBO for the TFH was only 40.5% of the average intensity, while it was 49.3% and 199% for the PIFH and IFH respectively.

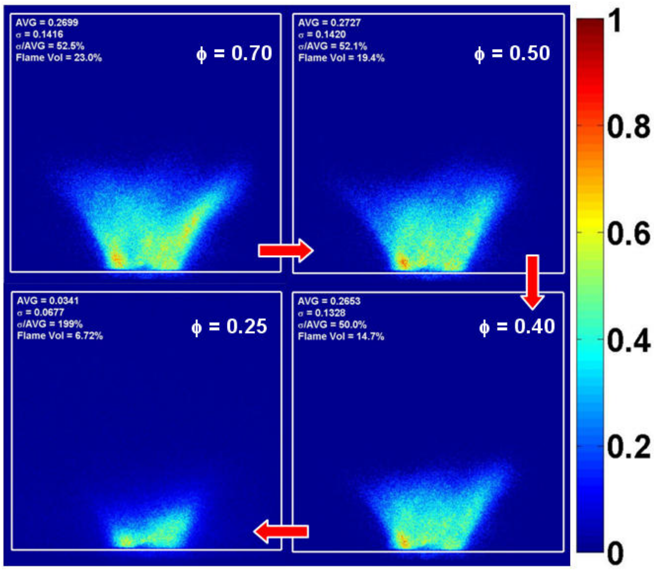

Figure 4: Chemiluminescence. ICCD imaging with 310nm filter, showing normalized flame intensity for IFH using diesel fuel with T3 = 622K and injector ΔP = 5.1%.

At very lean conditions the TFH has a reaction that appears completely distributed with no single anchor point and significantly homogeneous indicating a flameless mode of combustion. The PIFH also produces a fairly homogeneous flame distribution but is still stabilized by the forward stagnation point within the device. The reaction zone does not fully extend to the combustor dome, so this configuration appears to fall just short of a flameless type reaction. Unlike the TFH configuration, both the PIFH and IFH configurations leave "dead zones" in the corners of the combustor near the dome plate. Though still burning in a lean manner the IFH configuration retreats toward the forward stagnation point within the injection device and never approaches a flameless or distributed mode of combustion

All configurations have flame holding internal to the device at near stoichiometric conditions with the IFH and PIFH both having significant amounts of combustion occurring within the injection device even at very lean conditions. The device was designed with this intent for near stoichiometric, and no damage occurred to the injection device despite containing the combustion within. The high velocity, high swirl air in the forward most chamber, provide sufficient wall cooling to prevent the flame from damaging the chamber in the IFH configuration. The increased airflow through the forward swirler in the PIFH partial quenches the flame entering the forward chamber through along the negative axial velocity down the center of the venturi section. In the TFH configuration, with the secondary swirler of greatest effective area, CFD shows there is sufficient airflow to establish a stagnation point at the throat of the venturi section, preventing back-flow and therefore flame propagation into the forward most chamber. Therefore, at higher equivalence ratios the flame anchors at the throat of the venturi, while at lower equivalence ratios the flame enters a distributed mode. This is in contrast to the IFH where the flame is able to be pulled into the forward chamber where it is stabilized in a locally richer environment consisting of only the air from the secondary swirler.

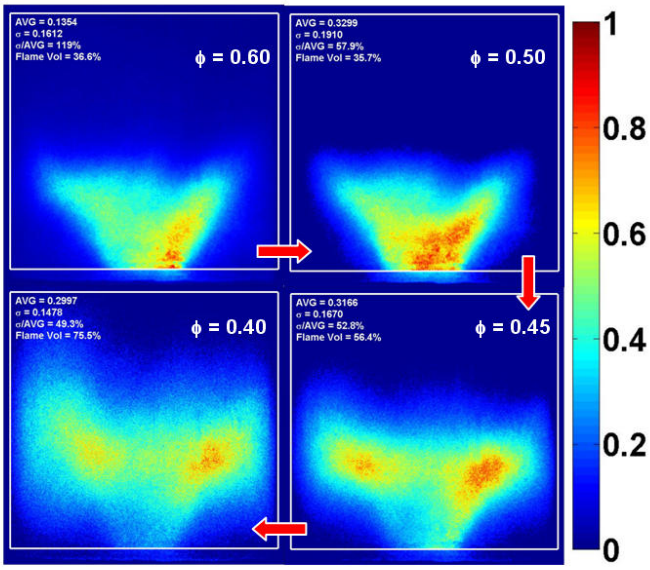

Figure 5: Chemiluminescence. ICCD imaging with 310nm filter, showing normalized flame intensity for PIFH using diesel fuel with T3 = 624K and injector ΔP = 3.0%.

The PIFH Based on the chemiluminescence images the reaction zone for the TFH appears to form flameless combustion similar to a well stirred reactor at lean conditions. Since the combustion chamber was a quartz tube, a pressure transducer could not be directly installed to measure combustion dynamics, however a microphone was placed approximately 3in downstream of the exhaust and 4in radially outward from the combustor wall. Unfortunately, in this location the measurement includes both combustion noise and the near field acoustics from mixing of the hot exhaust gases with cool ambient air. Despite this fact, some trends can be obtained from the acoustic measurements as shown in Figure 7. The IFH configuration has the lowest acoustic noise, which is possibly explained through mixing effects. Based upon the flame characteristics, the IFH has the most parabolic exit temperature profile, having a hot core but cooler wall temperatures so mixing with ambient air at the exit is less turbulent resulting in less near field noise levels.

The PIFH and TFH configurations start at higher noise levels as they have respectively broader flames, therefore hotter temperatures at the wall exit leading to a more turbulent shear layer between exhaust gases and ambient air. Both the IFH and

PIFH have slight increases in noise level as the combustion becomes leaner. In the case of the IFH this is possibly due to a lean instability mode, where the PIFH flame passes through a region in which the flame fluctuates from internally stabilized to only partial internally stabilized. To confirm this future work will need to be done with a metal wall combustor that permits attachment of a pressure transducer for direct measurement of combustion dynamics. For the TFH configuration the flame is broader at the higher equivalence ratios leading to the hotter near-wall temperatures and more energetic mixing with ambient air. It is important to note, though the near-wall temperature is higher, the core temperature is lower such that the exit temperature profile for the TFH configuration is flatter, especially at lower equivalence ratios. Though this configuration has a higher noise level at equivalence ratios near stoichiometric, the acoustic amplitude steadily decreases with declining equivalence ratio and therefore flame temperature. This corresponds to both a reduction in the turbulence of the mixing shear layer of the exhaust and to the transition into flameless mode of operation. It is currently unclear on how much of the noise level corresponds to exhaust mixing or combustion, again future studies will have to be done with an instrumented combustor to make this determination.

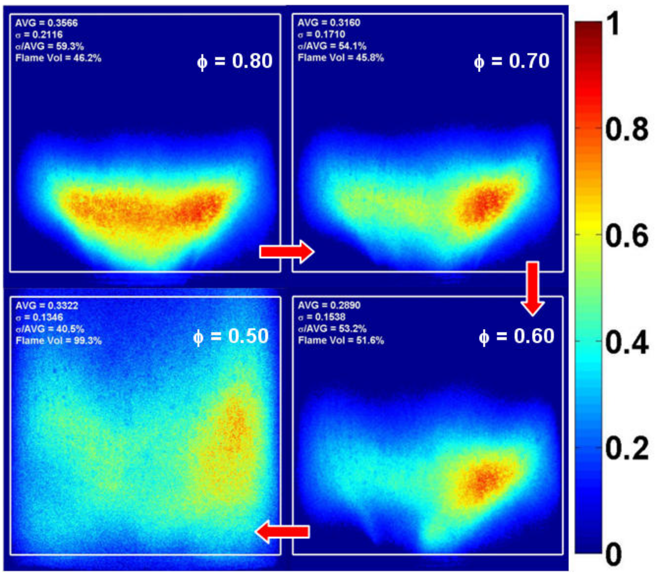

Figure 6: Chemiluminescence. ICCD imaging with 310nm filter, showing normalized flame intensity for TFH using diesel fuel with T3 = 563K and injector ΔP = 4.0%.

One of the biggest challenges to modern day gas turbine engines is reduction in the emission of environmentally damaging pollutants such as NO_X and CO. Figures 8 − 12 examine emissions of CO, NO_X, and UHC of the different injector configurations. Measurement in Figures 8 − 10 were taken with an emission sampling probe having a single sampling location at the exit of the combustor directly along the centerline. Measurements taken in Figures 11 and 12 were done with an emission rake probe having seven sample locations spaced 1in apart and centered about the combustor axis at the same axial position as the single point probe.

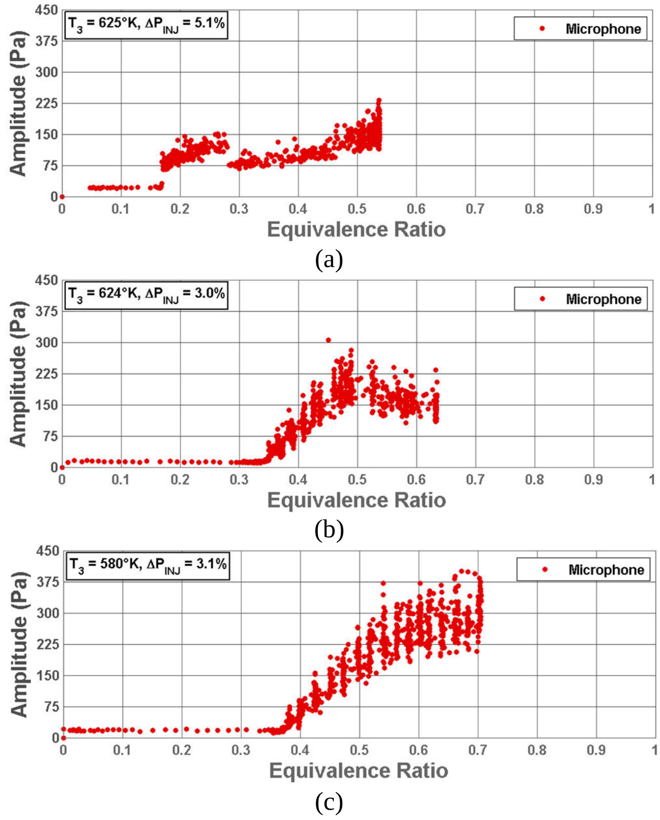

Figure 7: Near Field Acoustics. Plot of peak-to-peak amplitude of acoustic pressure measured downstream of combustor exit burning diesel fuel for configurations (a) IFH, (b) PIFH, and (c) TFH.

All emission measurements are corrected to 15% O_2 using Equations 1 − 3 from ref. [12] assuming the chemical formula of diesel fuel as $C_{10.8}H_{18.7}$ which sets the values in equations 1 and 2 to x = 10.8 and y = 18.7.

$$N_{Mix@\chi_{O_2}} = 4.76\left[\frac{x+\left(1-\chi_{O_2,act}\right)\frac{y}{4}}{1-4.76\chi_{O_2,act}}\right]-\frac{y}{4} \qquad \text{(Eq. 1)}$$

$$N_{Mix@15\%O_2} = 4.76\left[\frac{x+\left(1-.15\right)\frac{y}{4}}{1-4.76(.15)}\right]-\frac{y}{4} \qquad \text{(Eq. 2)}$$

$$\chi_{i,corr@15O_2} = \left(\frac{N_{Mix@\chi_{O_2}}}{N_{Mix@15\%O_2}} \right) \chi_{i,act} \qquad \text{(Eq. 3)}$$

Figure 8 illustrates emission for the IFH configuration which has the highest NO_X and CO concentration levels of the configurations based upon a single point measurement along the combustor centerline. The lowest NO_X value achieved was around 35ppm, though CO was near zero for a wide range of equivalence ratios. This is likely due to the strong re-circulation and relatively long residence time along the combustor centerline which allows sufficient time for completing the slow reaction of CO to CO_2. The UHCs for the IFH were zero over the entire range tested up until LBO, where the sudden and rapid jump in UHC levels corresponding to flame extinction. Though not shown, similar results were obtained for burning gaseous propane. It is interesting to note that the IFH was the only configuration for which the flame did not broaden with decreasing equivalence ratio and also resulted in the highest emission of harmful pollutants. Also of key interest is that the concentration traces of NO_X and CO match what is currently the expected standard for emission behavior: NO_X levels are proportional to equivalence ratio, increasing from low to near stoichiometric equivalence ratios. CO is inversely proportional to equivalence ratio: starting high at very low equivalence ratios and decreasing as stoichiometric conditions are approached. It will be seen that this traditionally standard trend does not hold true for all cases tested.

It can be seen from Figure 9 that the PIFH configuration had significantly lower concentrations of NO_X and CO compared to the IFH configuration as measured by the single point probe along the centerline. CO emissions were zero within the accuracy of the emission measurement device with NO_X below 10ppm below $\phi \approx 0.48$. But unlike the IFH configuration there were traces of UHCs in the exhaust of approximately 4ppm.

It can be seen in Figure 10 that the emissions for the TFH were similar to those found using the PIFH at lower equivalence ratios as shown in Figure 9. Unfortunately, the PIFH was not tested above approximately $\phi = 0.6$, so data for higher equivalence ratios is not available for comparison to the TFH. Carbon monoxide was practically zero until $\phi > 0.7$, and was still below 5ppm till the maximum tested condition of $\phi = 0.8$. This is where the emission trend breaks traditional expectations. In contrast to the IFH configuration that followed conventional systems, instead of CO increasing as the system gets leaner it follows NO_X and decreases. For the TFH NO_X was also very low, falling below 8ppm for $\phi < 0.6$. Unlike traditional systems that have a "sweet spot" where the opposing trends of NO_X and CO levels cross, both emissions parallel one another and both decrease with equivalence ratio. Therefore, continuing to go leaner lowers emissions of both CO and NO_X. Unfortunately, for the condition shown in Figure 10, UHC were higher for the TFH configuration than for the PIFH. For Figures 8 − 10 a single point emission probe was used along the combustor axis at the combustor exit plane. Figure 11 shows the same test condition as Figure 10, but using the 7 point emission rake, which is also used to obtain the data for Figure 12.

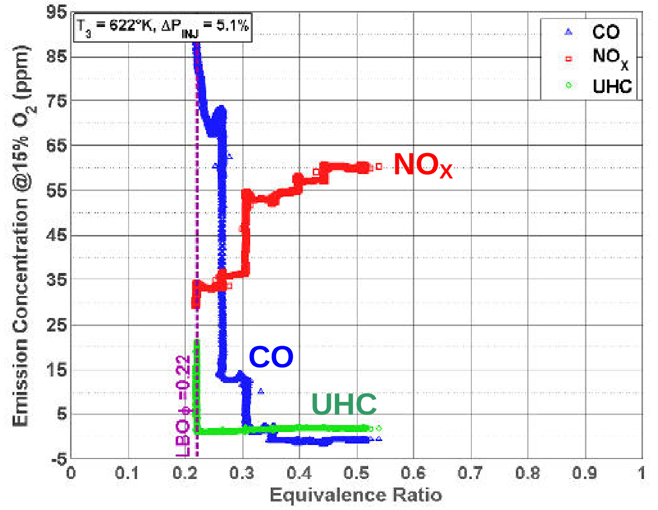

Figure 8: Emissions. Plot of corrected emissions of CO, NO_X, and UHC to 15% O_2 versus equivalence ratio collected by single point probe for IFH injector configuration burning diesel fuel.

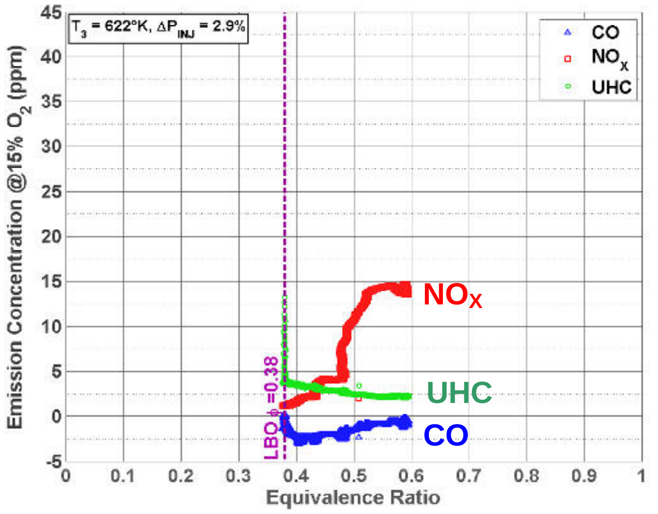

Figure 9: Emissions. Plot of corrected emissions of CO, NO_X, and UHC to 15% O_2 versus equivalence ratio collected by single point probe for PIFH injector configuration burning diesel fuel.

Comparing Figures 10 and 11 the NO_X values are slightly lower using the multi-point rake while CO concentrations are significantly higher. This indicates that the center region generates slightly higher levels of NO_X while the outer regions generate more CO. However, examining the data collected by the emission rake it can been seen that both NO_X and CO are less than 15ppm for $\phi < 0.65$ with NO_X falling to less than 5ppm and CO is practically zero for $\phi < 0.55$. UHC also significantly drops using the rake and maxes out around 14ppm instead of the 25ppm measured with the single point, indicating the majority of UHC production is in the center region. It is important to notice that the trends for CO and NO_X did not change between using the single point and the rake probes, confirming the parallel behavior of NO_X and CO as a real trend and not dependent upon measurement location.

Figure 12 illustrates the TFH emissions at a slightly higher pressure drop of 4.0% over the 3.0% seen in Figure 11, and is also the condition shown in the chemiluminescence images of Figure 6. Interestingly enough, the increase in re-circulation corresponding to higher pressure drop reduced the UHC to zero. Similarly, the average NO_X and CO values dropped by 2 to 3ppm, but LBO increased slightly. Other test conditions demonstrated that raising T_3 temperature also increased emission levels slightly, indicating the balance between mixing and chemical reaction rates to achieve the flameless mode of combustion and to maintain extremely low emission levels. Though not measured, another point of interest is that despite using a heavy hydrocarbon fuel such as diesel only a very fine film of carbon growth was found on the injector in a localized region.

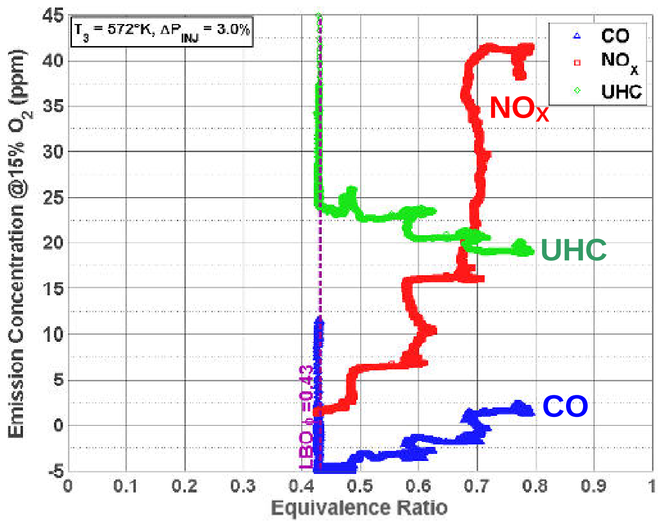

Figure 10: Emissions. Plot of corrected emissions of CO, NO_X, and UHC to 15% O_2 versus equivalence ratio collected by single point probe for TFH injector configuration burning diesel fuel.

After dozens of hours testing, for the TFH configuration especially, there were no heavy/thick deposits of carbon on the injector or combustor. None of the three configurations outlined in this paper produced any observable soot during testing. As seen in Figure 13, for the TFH configuration, the observed flame was purely blue and white even at equivalence ratios near stoichiometric. The red glow observed in the images at higher equivalence ratios comes from the radiant transmission from the heated quartz tube.

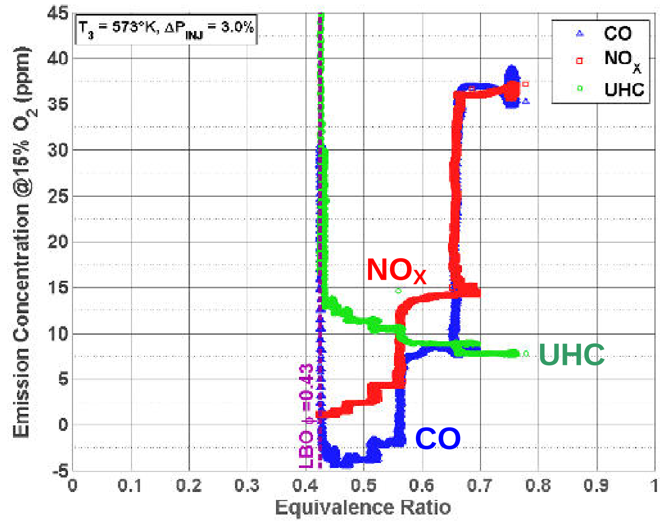

Figure 11: Emissions. Plot of corrected emissions of CO, NO_X, and UHC to 15% O_2 versus equivalence ratio collected by multipoint rake probe for TFH injector configuration burning diesel fuel.

Examining the plots of emission concentration in comparison to chemiluminescence images (flame shape) it can be seen that low emissions correspond to a distributed flame. Furthermore, the mode of flameless or distributed combustion was achieved from a sense of flame shape, acoustic levels, and emissions. More importantly for the purpose of the injection device, this was done within an architecture associated with current gas turbine combustor technology. One may notice that the flame images from both chemiluminescence and standard photography depict some asymmetry in flame shape. This is due to irregularities in fuel distribution which could possibly have contributed to delayed transition of the flame to a distributed reaction and lead to higher emission concentrations. This is not entirely unexpected in such an early stage of development and improving fuel distribution can be addressed in future designs, possibly leading to further performance improvements.

Figure 13 shows a strong glow emitted from the quartz tube at higher equivalence ratios, and is associated with significant amounts of thermal radiation transmitted from the quartz tube. This heat loss could possibly have contributed to premature lean-blow-out, so future studies will have to examine the effects of using a metallic wall combustor or thermal barrier coated combustor to determine how a more insulating wall with reduced heat loss impacts lean-blow-out limits, emissions, and acoustics. Based upon chemiluminescence the combustor length was more than twice as long as required to attain complete combustion. Again, future work will have to address these issues to confirm performance at increasingly more realistic test conditions. However, for an early study on feasibility in application toward a gas turbine engine, the experimental results are very promising and demonstrate good stability and emission capabilities without the complexity and cost associated with current in-practice technologies.

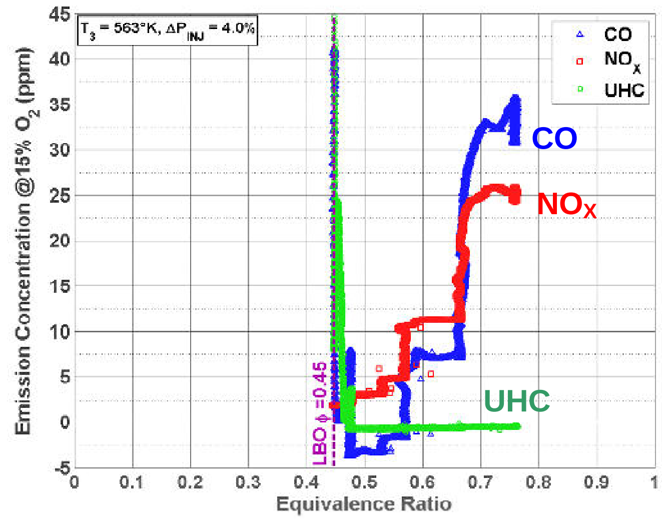

Figure 12: Emissions. Plot of corrected emissions of CO, NO_X, and UHC to 15% O_2 versus equivalence ratio collected by multipoint rake probe for TFH injector configuration burning diesel fuel.

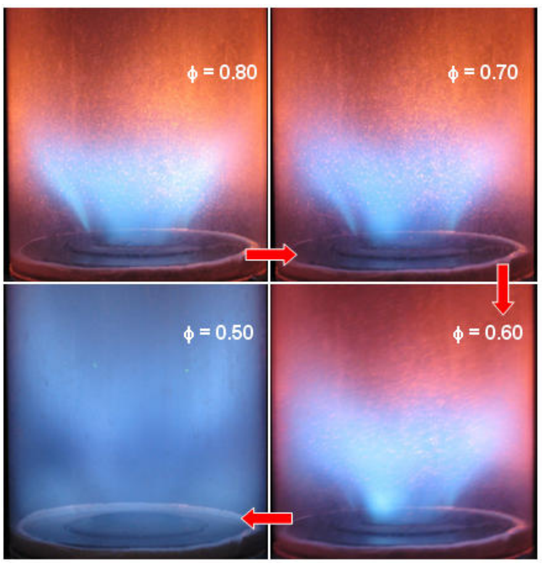

Figure 13: Combustion Images. Photographs of combustion at different equivalence ratios for TFH using diesel fuel with T_3 = 563K and injector ΔP = 4.0%.

NUMERICAL RESULTS

A numerical analysis was performed on the non-reacting flow field of the TFH configuration to determine the relative size and strength of the re-circulation zone. Non-reacting flow was chosen due to time constraints, though reacting flow may be studied in future analysis. A mesh of 7.2 million cells was run for a full scale 3D analysis using the RNG k-ε turbulence model with differential viscosity. Boundary conditions were 237kg/hr air mass flow rate at T_3 = 673.15K and P_4 = 1atm.

Figure 14 shows a side profile cross-section of the mean axial velocity with the positive flow direction being from bottom to top of the image. The exit of the injector is also shown for reference. The highest velocity can be seen exiting from the edge of the injector's inner diameter generating re-circulation zones both down the combustor centerline and in the corners. From the earlier chemiluminescence images, it can be seen that the flame holds to the inside of the high positive velocity layer (shown in Figure 14a & b in red), but as the system grows leaner and strength of the outer re-circulation zone increases the flame propagates into the outer region. Figure 14b shows a limited velocity scale of ±15m/s to better discern the regions of zero, positive, and negative axial velocities. From this image it can be estimated that the re-circulation zone starts to collapse between ℓ/D of 1.0 − 1.5, breaking down into smaller scale mixing, where ℓ is the axial distance from the combustor dome and D is the diameter of the combustor. This is at the limit of or slightly beyond the ℓ/D of 1.0 for which the chemiluminescence indicates complete combustion during flameless operation. Additional work will need to be done to more accurately determine the re-circulation zone collapse and its relationship to the size of the reaction zone for flameless combustion.

Cross sections through various axial positions of the flow field can be seen in Figure 15. Three regions of re-circulation can be seen at the injector exit: the inner core that extends upstream into the mixing device, a small middle annular zone around the injector lip, and the larger annular outer re-circulation zone near the combustor walls. Experimental results demonstrate the importance of the middle and outer re-circulation zones; as the combustion becomes leaner, swirl, and therefore re-circulation gets stronger. When the middle and outer re-circulation zones reach a critical strength a sufficient amount of fuel and combustion products are pulled upstream to facilitate combustion in these regions. Additionally, the stronger re-circulation results in rapid turbulent mixing which produces a homogeneous mixture of fuel, combustion products, and air in a sufficiently short time to sustain flameless mode of operation. Compared to the inner core re-circulation zone, the outer zone is considerably shorter in axial length around ℓ/D = 0.375, yet the velocities are similar to those in the core. Therefore, the residence time of the outer zone is considerably shorter, explaining why the emission concentrations of CO were higher in the outer zone, having less time to complete the conversion of CO to CO_2. This presents an interesting design challenge to achieve sufficient swirl strength to pull combustion gases and fuel upstream and mix rapidly with fresh air, but to also maintain sufficiently long residence time to allow the CO_2 reaction to complete. Additionally, the swirl must not be so strong as to go straight out, eliminating the outer re-circulation zone; instead a balance must be achieved between size and strength of the re-circulation.

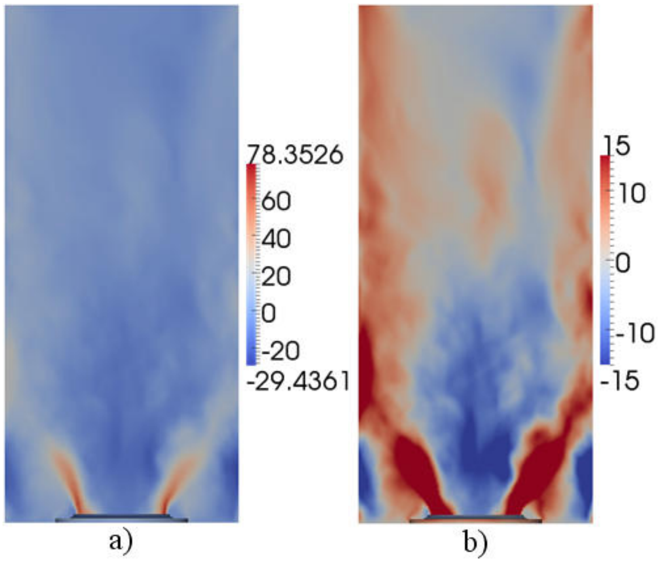

Figure 14: Contours of Axial Velocity. Profile cross-section of CFD results for mean axial velocity comparing a) full scale axial velocity and b) axial velocity clipped to ±15m/s to highlight the regions of re-circulation where positive axial velocity is bottom to top.

As seen with the side profiles, at approximately ℓ/D = 1.0 the inner core starts to break down and beyond ℓ/D = 1.25 smaller scale structures dominate the flow field. It is possible that small changes to combustor geometry can promote earlier collapse of the core re-circulation, which would result in accelerated mixing and faster break down of the large scale flow structures. This could lead to an overall shorter combustor design and higher combustion intensities while still achieving flameless combustion. Utilizing CFD to achieve tailored flow fields will be a crucial step in future development

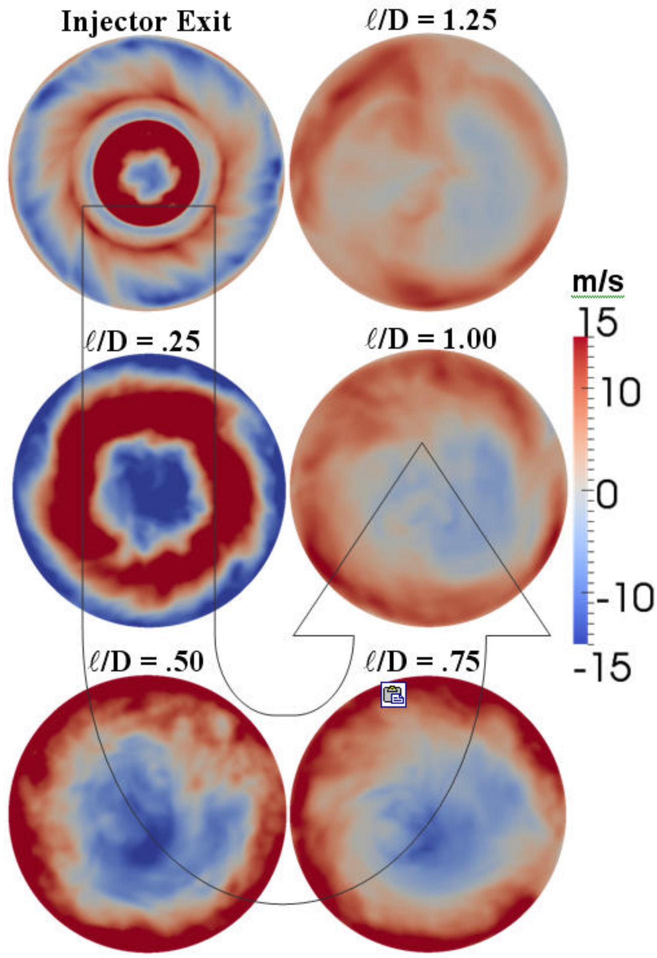

Figure 15: Velocity Cross-Section. Axial cross sections of CFD results for mean axial velocity where the velocity is clipped to ±15m/s to highlight the regions of re-circulation where positive axial velocity is bottom to top.

CONCLUSIONS

Work by Wünning et. al. [4] shows that flameless combustion is dependent primarily on re-circulation of hot combustion products above auto-ignition temperature and injector design that is suited to prevent formation of discrete flames whether attached or lifted. Work done by Gupta et. al. [1], Zinn et. al. [8], and Hamdi etl al [5] suggests flameless or distributed combustion can operate at combustion intensities above 50W/m^3/atm and elevated pressures suitable for both ground based and aerospace applications.

Though achieving flameless combustion in confined combustors such as those found in gas turbine engines, the current work has demonstrated the ability for more traditional, low weight, gas turbine combustor architecture to operate in a flameless regime while producing improved performance over a broad spectrum than that of classical or current lean burn technologies employed in gas turbines. Ultra low emissions were demonstrated including zero UHC from the range of LBO to $\phi = 0.8$, zero CO and $NO_X \leq 5ppm@15\%O_2$ for $\phi = 0.55$. Low near-field acoustics were demonstrated with a maximum of 300Pa peak-to-peak amplitude at $\phi = 0.8$, and decreased with equivalence ratio. For the best case configuration no instability was observed through flame dynamics or near-field acoustics, though additional work will be required to confirm this. Chemiluminescence imaging and photography illustrated efficient lean flame over a wide operating range with flameless mode occurring below $\phi = 0.45 – 0.55$ depending on inlet conditions. Though CFD results were for non-reacting flow, they indicate that the collapse of the central re-circulation zone is comparable to the axial position in which combustion completes while operating in flameless mode. CFD also correlated to emission distribution based upon residence time and CO concentrations between the inner and outer re-circulation zones.

These initial results are promising but future work still needs to be done to improve combustion intensity of the current system through refinement of both injector and combustor geometry. Further study on fuel placement and fuel split between primary and secondary circuits will also need to be done to increase turn-down ratio by lowering lean-blow-out to make the system more practical for power generation systems. Moving forward a key focus will be on examining how combustor geometry affects flame shape and emission levels. Additionally, it will be important to conduct high pressure tests to confirm performance capabilities at realistic operating conditions.

ACKNOWLEDGMENTS

Design and preliminary testing was conducted through Goodrich Engine Components Research Division. Extensive experimental testing was conducted at the University of Cincinnati with support from Russ DiMicco and Rodrigo Gomez.

REFERENCES

1. Arghode, Vaibhav K., Gupta, Ashwani K., Investigation of Distributed Combustion for Gas Turbine Application: Reverse Flow Configuration, 46th AIAA/ASME/ASEE Joint Propulsion Conference & Exhibit 25 - 28 July 2010, Nashville, TN
2. Levy, Yeshayahou, Levy, NOX Reduction in Gas Turbine Engines using Flameless Combustion, 24th Umbrella Symposium for the Development of Joint Cooperation Ideas, Jan 18-20, 2010, Forschungzentrum Julich, Germany
3. Erwann, Guillou, Cornwell, Michael, Gutmark, Ephraim, Application of "Flameless" Combustion for Gas Turbine Engines, 47th AIAA Aeropsace Sciences Meeting Including the New Horizons Forum and Aerospace Exposition January 5 - 8, 2009, Orlando Florida
4. Milani, Ambrogio, Wünning, Joachim G., New Pegenrative Burner for Flameless Oxidation in Radiant Tubes, UniversitâDegli Studi Di Napoli "Federoc II" April 26 - 28, 2009, Renningen, Germany
5. Hamdi, Mohamed, Benticha, Hmaïed, Sassi, Mohamed, Comparison and Parametric Study of Flameless Oxidation in a Gas Turbine Using Two Kinetics Mechanisms, American Journal of Environmental Sciences, 4 (5): 535-543, 2008
6. Guoqiang, Li, Gutmark, Ephraim, Stankovic, Dragan, Overman, Nick, Cornwell, Michael, Fuchs, Laszlo, Vladimir, Milosavljevic, Experimental Study of Flameless Combustion in Gas Turbine Combustors, 44th AIAA Aerospace Sciences Meeting and Exhibit, January 9 - 12, 2006, Reno Neveda
7. Murer, Sébastien, Pesenti, Barbara, Lybaert, Paul, Simulation of Flameless Combustion of Natural Gas in a Laboratory Scale Furnace, Turkish Journal of Engineering and Environmental Science 30 (2006), 135-143
8. Zinn, B.T., Neumeir, Y., Seitzman, J., et. a;. 2005 NSAS/DoD UAPT Program Review, 2005 Annual Reivew, May 11 - 12, 2005, Columbus, OH
9. Cavaliere, Antonio, de Joannon, Mara, Mild Combustion, Progress in Energy and Combustion Science 30 (2004) 329-366
10. Levy, Yeshayahou, Principle and Practice of the Low NOx FLOXCOM Gas Turbine Combustor, The Turbo and Jet Engine Laboratory
11. Sankaran, V., Gopalakrishnan P., Undapalli, S., Parisi, V., Seitzman J., Menon, S., A LES Investigation of a Stagnation Point Reverse Flow Combustor, 41st AIAA/ASME/SAE/ASEE Joint Propulsion Conference & Exhibit 10 - 13 July 2005, Tucson, AZ
12. Turns, Stephen R., An Introduction to Combustion Concepts and Applications. McGraw Hill 2000

